URI ARIELI

ULTRA BROADBAND OPTICAL RESPONSE OF LOCALIZED SURFACE PLASMON RESONANCES WITH DEEP SUB-WAVELENGTH RESOLUTION

ULTRA BROADBAND OPTICAL RESPONSE OF LOCALIZED SURFACE PLASMON RESONANCES WITH DEEP SUB-WAVELENGTH RESOLUTION

Ultrafast Phenomena at the Nanoscale

URI ARIELI

Physics Department
Faculty of Exact Sciences
Tel Aviv University
March 2017

Uri Arieli: *Ultra Broadband Response of Localized Surface Plasmon Resonance with Deep Sub-Wavelength Reolution,* Ultrafast Dynamics on the Nanoscale, ©

ABSTRACT

Investigating physics on the length scales of nanometers (10^{-9} meter) and time scales of femtoseconds (10^{-15} second) requires employing state-of-the-art instruments in order to overcome the challenges of these spatio-temporal orders of magnitudes. The scattering-Scanning Nearfield Optical Microscope (s-SNOM) and the femtosecond laser have been previously shown to enable measurements which surpass the spatial diffraction limit and the electronic circuits' time response, respectively, allowing to explore the nano-femto world.

In my thesis I show how the femtosecond laser and the s-SNOM can be incorporated in order to measure ultrafast phenomena on the nanoscale. Following the fabrication and far-field optical characterization of gold nanostructure, I employed the s-SNOM and the femtosecond laser in order to investigate the ultrabroadband optical response of gold nanostructures, mapping the hot spots as well as the full spectrum of the nanostructure. Also, I explain theoritically how these spectral measurement can be transformed into the time domain, yielding temporal resolution higher than the single cycle.

ACKNOWLEDGMENTS

This work, which scopes two years of my work during my M.Sc degree could not have come to an end without the appropriate guidance, consultation and assistance of others.

I would like to thank my supervisor, Dr. Haim Suchowski, for guiding me throughout these years.

Setting up simulations and experimental apparatuses could not have happened without the help of the Femot-Nano group members. Special thanks go to Dr. Michael Mrejen, who instructed me in construction of optical setups, as well as in the fine art of s-SNOM measurements.

CONTENTS

1 INTRODUCTION 1

2 THEORETICAL BACKGROUND 3
  - 2.1 Plasmonics 3
    - 2.1.1 Plasmons 3
    - 2.1.2 Localized Surface Plasmon Resonance (LSPR) 5
  - 2.2 Nearfield Microscopy 7
    - 2.2.1 Atomic Force Microscopy 8
    - 2.2.2 scattering Scanning Nearfield Micrscope (s-SNOM) 8
  - 2.3 Ultrafast Phenomena 11

3 EXPERIMENTAL APPARATUS 15
  - 3.1 Simulations 15
  - 3.2 Fabrication 16
  - 3.3 Far-field Characterization 16
  - 3.4 Nearfield Characterization with the s-SNOM 16
    - 3.4.1 Continuous Wave (CW) Measurements 17
    - 3.4.2 nano-FTIR Measurements 18

4 ULTRAFAST MEASUREMENT FASTER THAN THE SINGLE-CYCLE - THEORY 21
  - 4.1 Time Dynamics Information in the Interferogram 22
  - 4.2 Possible Applications 23
  - 4.3 Missing Information and Errors 24
    - 4.3.1 Missing Information due to Non-linear Processes 24
    - 4.3.2 FROG Spectral Phase Retrieval 24
    - 4.3.3 Errors Originating in the Experimental Apparatus 25
  - 4.4 Preliminary Results - Ultrafast Dynamics in LSPRs 25
    - 4.4.1 Time Domain Simulations of Coupled LSPRs Dynamics 25
    - 4.4.2 Experimental Measurements of Coupled Orthogonal Bars 26

5 SUMMARY AND OUTLOOK 31

BIBLIOGRAPHY 37

ACRONYMS

s-SNOM	scattering-Scanning Nearfield Optical Microscope
LSPR	Localized Surface Plasmon Resonance
SPP	Surface Plasmon Polariton
FROG	Frequency Resolved Optical Gating
FTIR	Fourier Transform Infrared
TEM	Transmission Electron Microscope
AFM	Atomic Force Microscope
CW	Continuous Wave

1

INTRODUCTION

Ancient Greeks and Romans showed more than 1,000 years ago that macroscopic features of a material can be influenced by it's micrscopic properties. Without the physical understanding they have created the famous *Lycurgus Cup*. This manipulation of matter on the nanoscale can also be seen in the colorful windows of ancient churches constructed in the middle ages, long before the appearance of modern science. These phenomena were not understood until 1908, when Gustav Mie published his paper, "*Contributions to the optics of turbid media, particularly of colloidal metal solutions*" [1], explaining how microscopic features of metal particles, with sizes below the relevant wavelength, can influence macroscopic features such as the interaction of light and matter (or in layman's words - colors). This theory is now recognized as "*Mie Scattering*" .

Mie's work has shown that by controlling the sub-wavelength properties of matter, such as shape, size, orientation and distance from other optical metamaterials (which results in optical coupling), we can recieve a wide range of optical response from the same material, from electric field enhancement to shifting the resonance wavelength of a material.

These metamaterials were suggested as candidates for different applications: detectors [2], bio-sensors [3], cancer treatments [4], single-molecule detection [5], optical computing [6], non linear optical processes [7] and photo-voltaic cells [8].

Hence, various forms of optical-metamaterials were heavily explored [9][10]. By shining a Continuous Wave (CW) laser, or an incoherent broadband light, on nanostructures, the material's absorbance, scattering, polarization, and other properties of the Electromagnetic response, can be measured for each wavelength separately. Using a near-field micrscope, the electric near-field spatial distribution can be measured as well. Yet, recieving a temporal picture of these materials is more complicated. Since these materials operate in the visible to NIR frequencies, measuring those processes will require detector with temporal resolution of femtoseconds, well beyond the capability of electrical circuits, which operate mostly on the ~ 1 nanosecond time scales. To tackle the problem of limited temporal resolution, researchers provided a variety of solutions, such as pump-probe experiments.

In this work, we used an ultrafast 6 femtosecond Laser and scattering-Scanning Near Field Microscope (s-SNOM) on various nanostructures in order to spectrally characterize them with a spatial resolution of 25 nanometer. Furthermore, we suggest a method to image the nearfield of the nanostructures with temporal resolution higher than the single cycle.

Chapter 2 (*Theoretical Background*) presents the theoretical background for light and matter interaction on the nanoscale. An introduction to nearfield microscopy and ultrafast measurement is presented. Chapter 3 (*Experimental Apparatus*) presents experimental work done with gold nanostructures - numerical simulations, fabrication, far-field characterization and nearfield characterization using the s-SNOM. Chapter 4 (*Temporal Measurements Faster than the Single Cycle - Theory)* presents a theory we have devised, which we claim will enable to transform nano-FTIR measurements to the time domain, achieving a sub-cycle temporal resolution in the near field domain.

2

THEORETICAL BACKGROUND

In this chapter, we discuss the three basic layers that set the ground for my research work: plasmonics, near-field microscopy and ultrashort laser sources.

2.1 PLASMONICS

The interaction of light with metal results in the excitation of different physical modes, such as phonon-polaritons, plasmon-polariton, exciton-polariton and more. In this section we introduce the plasmon and discuss it's properties.

2.1.1 *Plasmons*

Plasma oscillations in metals, referred to as plasmons when quantized, are the collective oscillations of free electrons in metals. When a light strikes a metal, the photons are coupled to the metals' electrons, yielding a plasmon-polariton. This coupling results in scattering and absorption of electromagnetic energy.

The metal's reaction to the incident electronmagnetic radiation is dictated by Maxwell's equation in the absence of free charges. These equations give the known relations $\vec{\nabla} \cdot \vec{D} = 0$ and $\vec{\nabla} \times \vec{H} = \frac{1}{c}\partial_t \vec{D}$, where $\vec{D}(\omega) = \epsilon(\omega)\vec{E}(\omega)$ and $\mu(\omega)\vec{H}(\omega) = \vec{B}(\omega)$. $\epsilon(\omega)$ and $\mu(\omega)$ are known as the permitivitty and the permeability, respectively. For most materials, $\mu(\omega) = 1$.

Extracting the permitivitty, $\epsilon(\omega)$, experimentally or theoreticly, is a matter of great interest, as it contains information on the bandstructure of the electrons in the metal. Simplistic models, such as Drude Model and Lorentz Model, are used in order to simplify calculations.

These models assume that the electrons in the metal can be approximated as classical objects experiencing the Lorentz force. Assuming the electrons are bound by some potential, which is approximated as a force of a spring for small displacement, we derive the following equation:

$$m_e\ddot{x}(t) + m_e\gamma\dot{x}(t) + m_e\omega_B^2 x(t) = -eE(t)$$

Transforming to the frequency domain we can extract the spectral amplitude of the oscillation as:

$$x(\omega) = \frac{-eE}{m_e} \frac{1}{\omega_B^2 - \omega^2 + i\gamma\omega}$$

Using the relation $\vec{D} = \epsilon(\omega)\vec{E} = (1 + \chi(\omega))\vec{E}$, where $\chi = P/E$, and $P = -nex(\omega)$ is the dipole-moment density we get:

$$x(\omega) = \frac{-eE}{m_e} \frac{1}{\omega_B^2 - \omega^2 + i\gamma\omega} \tag{2.1}$$

Examining equation 2.1, we can see that the material's response to electromagnetic radiation resemble a Lorentzian around ω_B, with full width half maximum (FWHM) of γ. Furthermore, we can observe that the electrons oscillate with a spectral phase to the exciting electric field:

$$\phi(\omega) = tg^{-1}\left(\frac{\gamma\omega}{\omega_B^2 - \omega^2}\right)$$

In metals, the permitivitty function can be usually approximated by contribution of free electrons ($\omega_B = 0$) as well as bounded electrons and ionic background, yielding a final expression which sums all those contributions:

$$\epsilon(\omega) = 1 + \epsilon_{ion} - \frac{ne^2}{m_e} \frac{1}{\omega^2 - i\gamma\omega} + \frac{ne^2}{m_e} \sum_{\omega_B} \frac{1}{\omega_B^2 - \omega^2 + i\gamma\omega}$$

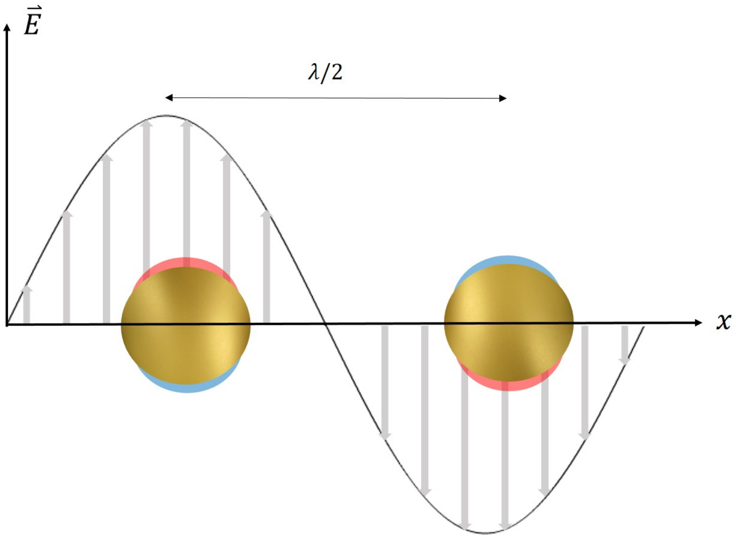

Figure 2.1: Schematics of electrons' oscillations in metallic nanoparticles due to excitation by electromagnetic radiation.

2.1.2 *Localized Surface Plasmon Resonance (LSPR)*

While exciting bulk metal creates a traveling excitation of electrons along the metal's surface (called Surface Plasmon Polariton (SPP)), when the metal is spatially confined, on the order of size less than the incident wavelength, a different phenomenon occurs - a standing wave of charged density is formed, which is called Localized Surface Plasmon Resonance (LSPR). A simple analytical example of an LSPR can be demonstrated by solving Maxwell's equations for a metallic sphere in a uniform electric field.

By setting p as the induced dipole moment, and E as the incident electric field, the polarizability $\alpha = \frac{p}{E}$ can be extracted. Solving for the appropriate boundary conditions, an analytical expression can be derived for the polarizability[11]:

$$\alpha = R^3 \frac{\epsilon_m - \epsilon_h}{\epsilon_m + 2\epsilon_h}$$

A more general solution of α, which applies to any kind of ellipsoid in the dipole limit (R_1, R_2, $R_3 \ll \lambda$) is given by the known formula:

$$\alpha = \frac{R_1 R_2 R_3}{3} \frac{\epsilon_m - \epsilon_h}{L_1(\epsilon_m - \epsilon_h) + \epsilon_h}$$

where R_1 is the ellipsoid's axis parallel to the polarization's direction, R_2 and R_3 are the remaining ellipsoid's axes and L_1, named the Depolarizing Factor, is given by:

$$L_1 = \frac{1}{2} \int_0^\infty \frac{R_1 R_2 R_3 ds}{(R_1^2 + s)^{3/2}(R_2^2 + s)^{0.5}(R_3^2 + s)^{0.5}}$$

Using Rayleigh's scattering and the local Watt law ($P = -\vec{J} \cdot \vec{E}$) we can calculated the absorption and scattering cross sections, respectively:

$$C_{sc} = \frac{8\pi}{3}(\frac{2\pi}{\lambda})^4 |\alpha|^2$$

$$C_{abs} = 4\pi(\frac{2\pi}{\lambda}) Im\{\alpha\}$$

The Extinction Cross Section can be simply calculated by summing the different cross sections.

Two main interesting characteristic of the LSPRs are the ability to control the resonance' wavelength by manipulating the nanostructure's geometry, as well as nano-confinement of the electric field in hotspots around the nanoparticles.

The shift in the wavelength of the resonance occurs due to an effective change in the pressure of the free electrons *"fluid"*, just as changing the length of a guitar string changes it's fundamental frequency [12]. Furthermore, realizing structures that are more complex than simple ellipsoids, such as Split Ring Resonators, can introduce more than one resonances, and different resonances in different polarizations.

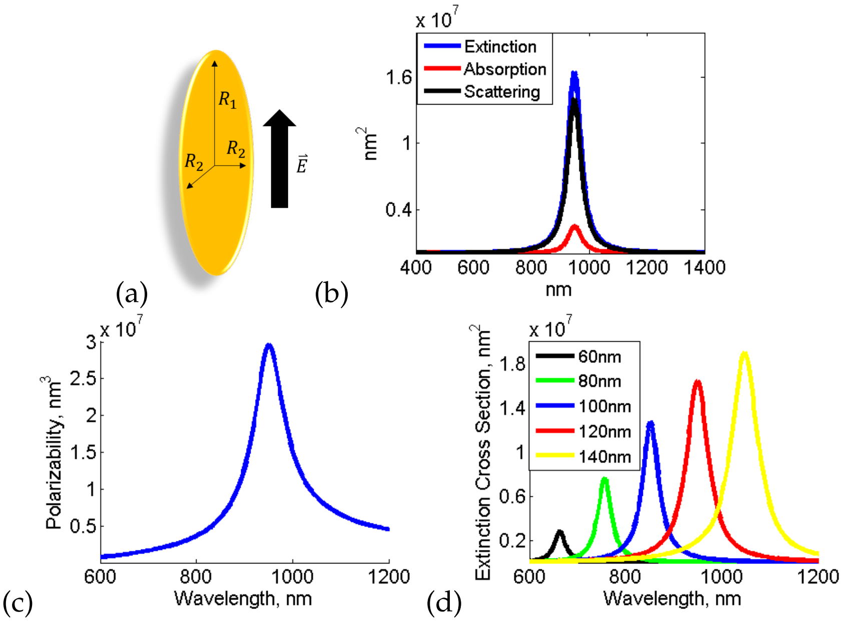

Figure 2.2: (a) A gold nano-ellipsoid in a uniform electric field. (b) Analytical result for the different cross sections of a 120 nm long nano-ellipsoid. (c) The polarizability (α) of a 120 nm long nano-ellipsoid. A small red shift of $\sim 1.5nm$ can be observed from the extinction cross section. (d) The Extinction Cross Sections of different nano-ellipsoids with different major axis (60-140 nm).

The enhancement of the near field in hot-spots in the proximities of the nanostructures is another important characteristic of the LSPRs. This enhancement is usually on the order of magnitude of a few dozens (around ~ 30 for a nano-ellipsoid) of the exciting electric field, and is spatially confined to a few dozens of nano-meter, deep into the sub-wavelength regime. High non-linear effects can come about due to this enhancement.

Tunable resonance and huge electric field enhancement made Optical Metamaterials promising candidates for many possible applications such as sensors [2], bio imaging [3], single molecule detection [5], optical computing [6] and more .

COUPLED LSPRS

While when the distance between the nanoparticles is much larger than the typical size of the nanoparticle the nano-particles interact with the electromagnetic field independently of eachother, when the distance between the particles drops down to the order of magnitude of the nano-particles' size, they start to interact with eachother via their induced electric near field.

This interaction gives rise to the hybridization of modes[13] as well as nano confinement of the electric field, thus making systems of coupled LSPRs as candidates for applications such as nano-rulers and single molecule detection[14], which is made possible with electric field enhancement on the order of magnitude of $\sim 10^3$.

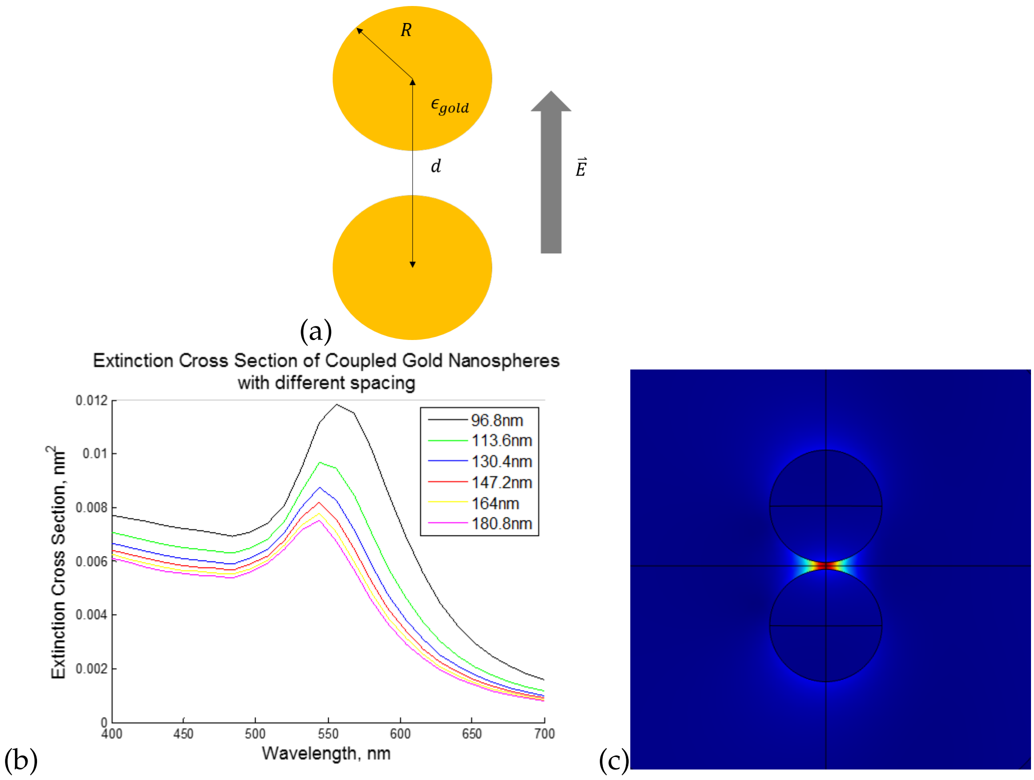

Figure 2.3: Numerical simulations (COMSOL Multi-Physics) of coupled gold spheres, with radius of 40nm (R) and varying spacing (d). (a) Two coupled spheres in an electric field. (b) A red-shift in the extinction Cross Section can be observed as the separation between the spheres decreases. (c) Electric field enhancement between two nanospheres. In the resonant wavelength, when the separation between the nanospheres is 4nm, the electric field is ~60 times higher than the incoming electric field.

2.2 NEARFIELD MICROSCOPY

The Nearfield Microscope consists of a conductive Atomic Force Microscope (AFM) tip with a ~30nm radius of curvatue, which enables probing the sample at deep sub-wavelength resolutions, allowing us to extract topographical image, as well as the intensity of the electric field, it's spectrum and phase. The next section introduces it's mode of operation, as well as the different measurements modes it contains.

2.2.1 *Atomic Force Microscopy*

The AFM allows us to extract a 2-dimensional topography of a sample with sub-wavelength resolution. The AFM main components consist of a tip, a cantilever, a laser and a photodiode (See figure 2.4). The cantilever is modulated via a lock-in at it's eigen-freuquency (around ~200kHz in our system) at a constant amplitude. The tip is then brought into proximity with the surface. When repulsive forces from the surface deflect the tip, the cantilever is deflected as well, causing to the deflection of the AFM laser, which is recorded in the photodiode. By measuring the deflection of the laser for each point in space we can create a 2-dimensional topographical map of our sample, with a resolution which depends solely on the tip's width.

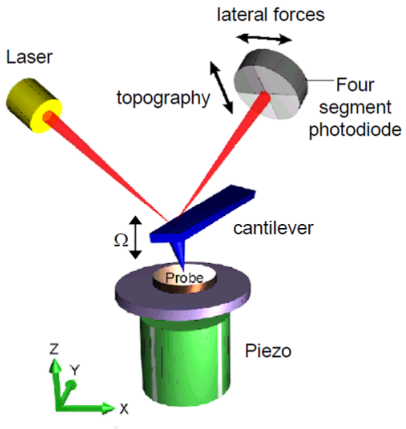

Figure 2.4: Schematics of the AFM operation mode. Image taken from reference [15].

2.2.2 *scattering Scanning Nearfield Micrscope (s-SNOM)*

The principles of the s-SNOM are quite similar to those of the AFM - using an ultra-thin tip in order to extract sub-wavelength information from the sample (see figure 2.5).

The nearfield of the sample, excited by a laser source, causes to excitation of the conductive tip. The polarization of the tip causes a scattering event which is detected in the far-field by a photodiode.

Signal Extraction

The main difficulty in operating the s-SNOM is filtering the background noise - while the tip is only ~30nm wide, the laser beam

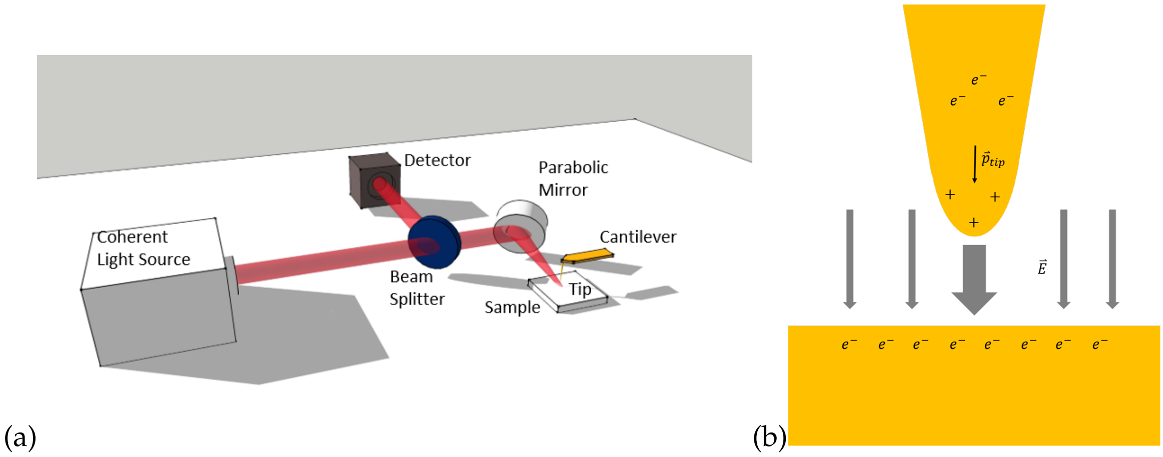

Figure 2.5: Schematics of the s-SNOM operation. (a) The general configuration of an s-SNOM. (b) Zoom in in on the tip-sample interaction. The electric nearfield of the sample induces a polarization in the s-SNOM's tip ($\vec{p}_{tip}$), leading to the scattering of an electromagnetic wave from the tip. The wave is then collected with a parabolic mirror and detected with a photodiode.

spot's size is diffraction limited and on the order of magnitude of hundreds of nanometers. Thus, most of the incoming signal is not the pure nearfield which we wish to extract. This problem is solved by modulating the tip's height at the cantilever's mechanical eigenfrequency. This modulation allows us to separate the pure nearfield signal, which will now be modulated at a known frequency, from the background noise. Furthermore, because that the nearfield of the nanoparticle decays as quickly as $\sim \frac{1}{r^3}$, by extracting the high harmonics of our signal, with regard to the modulation frequency, we may obtain an image with improved signal to noise ratio.

Pseudo-Heterodyne Detection

Thus far, we have explained how the intensity of the nearfield can be mapped using the s-SNOM. Yet, there's more information in the nearfield region - the optical phase.

Phase information can be retrieved by incorporating an asymmetric interferometer (either Michelson-Morley or Mach-Zehnder) to the s-SNOM. By modulating the reference arm mirror's position and creating an interference pattern the optical phase of the nearfield can be extracted, as well as the intensity, allowing us to fully re-create the optical dynamics of our sample. More information can be found in reference [16].

nano-FTIR

Pseudo-heterodyne detection scheme allows us to fully characterize the nearfield dynamics of our sample, but it can do so only for a single CW light source at a time. The nano-Fourier Transform Infrared (FTIR) module (see figure 2.6) enables us to measure the nearfield spectrum with a broadband light source.

The nano-FTIR operates in the following way: An electromagnetic pulse is split into two by a beam splitter. The signal beam (S) interacts with the sample, and the reference beam (R) travels through air only. Both beams are later recombined in the beam splitter and their interference measured in a photodiode.

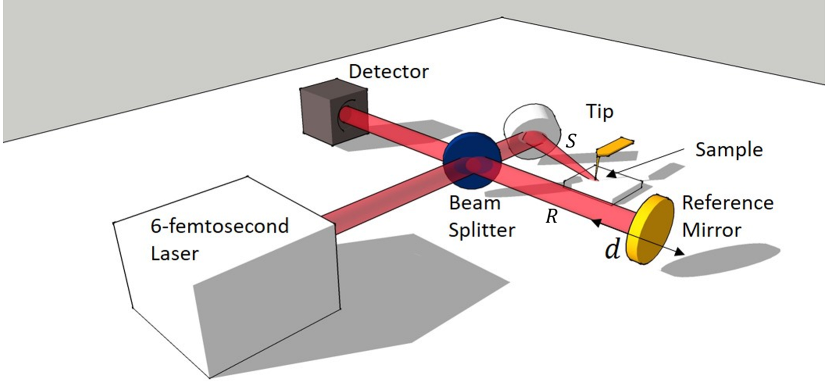

Figure 2.6: Schematics of the nano-FTIR. The R and S beams represent the Reference and Signal beams, respectively.

Let us assign $S = \sum_k S_k e^{-i\omega_k t}$ and $R = \sum_k R_k e^{-i\omega_k t} e^{ikd}$ as the signal beam and reference beam, respectively. The quantity which will be measured in the detector will be the intesity, $I(d,t)$:

$$I(d,t) \propto \sum_{k,k'} (S_k e^{-i\omega_k t} + R_k e^{i(-\omega_k t + kd)})(S^*_{k'} e^{i\omega_{k'} t} + R^*_{k'} e^{-i(-\omega_{k'} t + kd)}) =$$

$$|S|^2 + |R|^2 + \sum_{k,k'} S_k R^*_{k'} e^{-i(\omega_k - \omega_{k'})t} e^{-ikd} + R_k S^*_{k'} e^{-i(\omega_k - \omega_{k'})t} e^{ikd}$$

Let us neglect the DC components and assign $\phi_{p,k}$ as the spectral phase of the pulse (more information on $\phi_{p,k}$ can be found at section 1.3 Ultrafast Phenomenta, equation 2.5). Since we measure only the average intensity of the pulse, our detector will show:

$$< I(d) >_t = \lim_{T \to \infty} \frac{1}{T} \int_0^T I(d,t) dt \propto \sum_k |S_k R_k| (e^{i(\phi_{p,k} + \phi_{s,k} - \phi_{p.k} - \phi_{r,k})} e^{-ikd} + c.c) =$$

$$\sum_k |S_k R_k| \cos(kd + \phi_{r,k} - \phi_{s,k}) \propto \sum_k |S_k R_k| e^{i(\phi_{r,k} - \phi_{s,k})} e^{ikd}$$

Since no interaction occurs in the reference' arm, we can take $\phi_{r,k} = 0$, giving the result:

$$< I(d) >_t = \sum_k |S_k R_k| e^{-i\phi_{s,k}} e^{ikd} \tag{2.2}$$

$< I(d) >_t$ is called the *Interferogram*. The k_{th} Fourier component of $< I(d) >_t$ is proportional to $|S_k R_k|$, and it's phase is the phase which was contributed to the S beam by the sample. More information on FTIR mathematics can be found in reference [17].

2.3 ULTRAFAST PHENOMENA

Many fundamental proccesses in nature, such as molecular vibrations and the movement of electrons in metals or the oscillation of electromagnetic waves, occurs on time scales of picoseconds (10^{-12} seconds) or femtoseconds (10^{-15} seconds). As such, investigating the dynamics of these proccesses requires a measurement tool with a shutter time faster than the measured event. These shutter times are unachievable by modern electronics, which usually do not operate faster than nanoseconds. A shutter time of different physics needs to be employed.

Ultrafast Laser

One way of constructing an ultrafast shutter is using a broadband electromagnetic pulse. The shutter time of the pulse can be approximated by Heisenberg's Uncertainty principle: $\triangle\omega\triangle t \leq \frac{1}{2}$. This means that the greater the bandwidth of the pulse the faster the shutter can be. Conventional methods include pump-probe experiments, in which the sample is excited by one pulse (pump) and probed with the other (probe). The response is measured for different delays between the pump and probe, enabling the study of time dependent ultrafast dynamics.

Furthermore, the wide range of frequencies contained in one pulse enables us to use it as a white light source, fully recording the spectrum of a sample in a single pulse.

In this work we used a 6fs Ti:sap laser with a bandwidth of 650-1100nm.

Propagation of Ultrafast Pulses

In vaccum, Electromagnetic waves all travel with uniform speed, the speed of light. In the presence of a dielectric medium which interacts with the electromagnetic radiation, each frequency component travels with a different speed. When addressing dynamics excited by a broadband pulse, even sparse medium such as air gives rise to time-dependent dynamics in the pulse′ electric field. These effect gain importance when the effective refractive index of air, $n(\omega)$, can no longer be approximated as a constant throughout the relevant frequency range of the pulse.

Assuming the pulse can be described as Gaussian pulse, we can write the following expression:

$$E(t) = E_0 \exp(-\frac{t^2}{\tau_0^2}) \exp(-i\omega_0 t)$$

Let us first assume that the spectral phase acquired can be approximated with a 2^{nd} order Taylor series in the following way:

$$\phi(\omega) = \phi_0 + \phi_1(\omega - \omega_0) + \frac{1}{2}\phi_2(\omega - \omega_0)^2 + O((\omega - \omega_0)^3) \quad (2.3)$$

We can then calculate the final temporal dynamics of the pulse in the following way:

$$E(t) = E_0 \exp(i\omega_0\phi_1) \exp(-i\omega_0 t) \sqrt{\frac{\tau_0^2}{\tau_0^2 - 2i\phi_2}} \exp(-\frac{t^2\tau_0^2}{\tau_0^4 + 4\phi_2^2} + 2i\frac{t^2\phi_2}{\tau_0^4 + 4\phi_2^2}) \quad (2.4)$$

Setting $\phi_2 = \beta_2 L$, where β_2 is the 2nd order correction for the wave-vector with respect to the frequency, the dependence of the pulse temporal width on the length of the medium can be directly extracted by assigning $\tau_{eff} = \sqrt{\tau_0^2 + 4\frac{\phi_2^2}{\tau_0^2}}$.

Looking back at equation 2.3 we can see that while the pulse is traveling in space it acquires a quadratic spectral phase. Representing this phase as a function of the wave-vector, we can define the spectral phase of the pulse in the following way:

$$\phi_{p,k} = \phi_0 + \beta_1(k - k_0) + \frac{1}{2}\beta_2 L(k - k_0)^2 + O((k - k_0)^3) \quad (2.5)$$

The ability to control the pulse temporal width enables manipulation of matter via non linear processes[18][19]. Compressed pulses, also known as Transform limited pulses, which have a temporal width that is determined by the Fourier limit, are used to conduct pump-probe experiments, in which the pulse temporal width is used as an effective shutter. For more information on ultrafast pulse-shaping see reference [19].

Experimental measurement of the dependence of the electric field in time of an ultrashort is a non-trivial task. The pulse can be between a few femtoseconds to a few picoseconds long - far faster than the fastest photodiode. This problem can be resolved by Frequency Resolved Optical Gating (FROG). FROG allows retrieval of the full information about an ultrashort pulse - amplitude and spectral phase. For more information see reference [20].

3

EXPERIMENTAL APPARATUS

This chapter overviews the numerical simulations and the experimental work conducted in order to realize the nano-FTIR measurement with a 25nm spatial resolution.

3.1 SIMULATIONS

Since the optical response of only the simplest of optical metamaterials can be solved analytically, numerical simulations have to be employed in order to understand responses in both the frequency and time domain in order to understand complex structures. In this part we will discuss results from COMSOL simulation in the frequency domain.

Predicting the Steady-State Response of Optical Metamaterials

Previous to fabrication of nanostructures, appropriate geometries need to be found, in order to adjust the LSPR to the relevant wavelength of interest.

Scattering experiments were designed in *COMSOL Multi Physics* in order to find the optical response properties (figure 3.1). The simulations predicted the transmission spectra of different gold nano-bars fabricated on a thin layer of ITO and glass.

Figure 3.1 shows the dependence of the transmission on the length of a gold nano-bar with thickness and width of 40nm. A clear redshift in the resonance can be observed for longer nanobars.

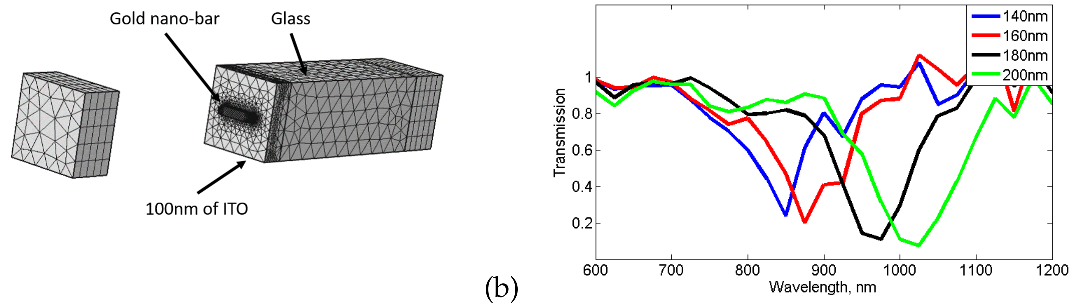

(a) (b)

Figure 3.1: (a) A COMSOL simulation of a gold nanobar, on a thin layer of ITO and glass. (b) The transmission of nanobars with different lengths (COMSOL simulation results).

3.2 FABRICATION

In order to fabricate different gold nanostructures, such as nanobars and nano-slits we employed Electron Beam Lithography. For more information, see the appendix.

3.3 FAR-FIELD CHARACTERIZATION

In order to characterize the nanostructures in the far-field, a Reflection-Transmission characterization setup was built. The setup employed two NIR achromatic Mitutoyo Objectives, 20X objective for the focusing of the light and 50X objective for the light collection. A lense was then placed after the collecting objective in order to create an image in the plane of an iris, where the sample's image could be filtered spatially. Filtered image would then go to various spectrometers, depending on the wavelengths of interest.

Figure 3.2 shows far-field measurement done on gold nanobars with different aspect-ratio. The expected redshift in transmission can be clearly observed, as the simulation predicts.

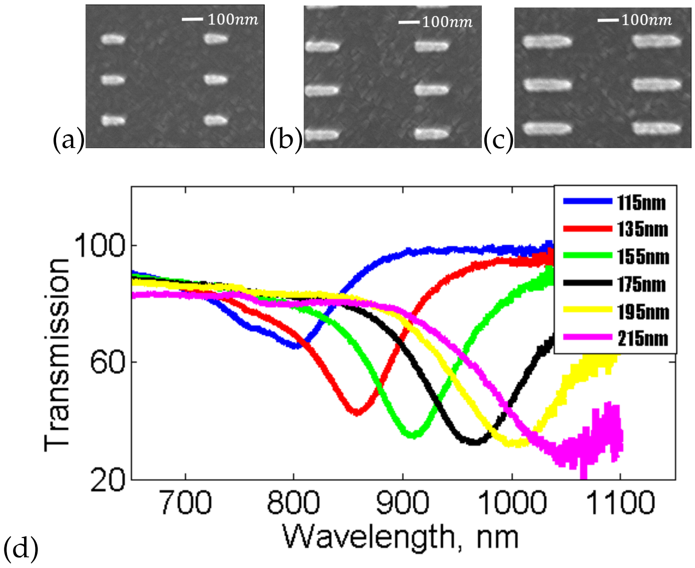

Figure 3.2: (a)-(c) SEM images of gold nanobars of different lengths. (d) Transmission spectra of gold nanobars with different lengths.

3.4 NEARFIELD CHARACTERIZATION WITH THE S-SNOM

Structures which showed optical response in relevant wavelengths were then inspected in the near-field with the s-SNOM. This sections presents results achieved both with CW laser, as well as the incorporation of the s-SNOM and the femtosecond laser.

3.4.1 *Continuous Wave (CW) Measurements*

Prior to incorporating the s-sNOM and the femtosecond laser, several CW measurements were conducted in order to investigate structures of interests. Measurements of intensity and phase were done in Reflection and Transmission modes.

Figure 3.3 shows a typical s-SNOM measurement of a gold nanobar using the pseudoheterodyne detection scheme (details on the detection scheme can found in Ocelic et al. [16]) , in response to excitation with a 1580nm CW. Sub-figures (b) and (c) show the amplitude of the optical signal and the optical phase, respectively. These images are then composed in sub-figure (d), confirming the existance of a dipole moment, induced by the electric field. A faint mirror image above the bar can be seen, due to imperfection in the probing tip.

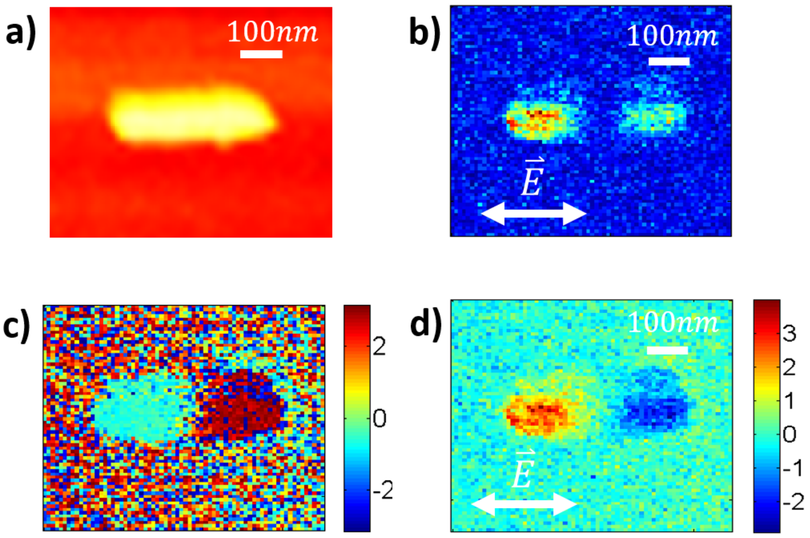

Figure 3.3: Inspecting a gold nanobar with the s-SNOM with pseudoheterodyne detection scheme. (a) AFM image of a 40nm-thick gold nanobar. (b) Nearfield Optical intensity. (c) Optical phase of the nanobar, in radians. (d) The real part of the electric field, reconstructed with the measured amplitude and the phase (a.u). Figure was created by taking the Optical signal intensity and multiplying it with the exponent of the phase times the imaginary unit.

Figure 3.4 shows the nearfield of a gold nano-slit, excited in the x-axis with a 633nm CW. The nano-slit is resonating in the x-axis, leading to what seems as propagation of free electrons along the surface of the gold. This observation concurs with long distance optical coupling between nano-slits in the frequency domain. Further measurements will be conducted in order to verify this result.

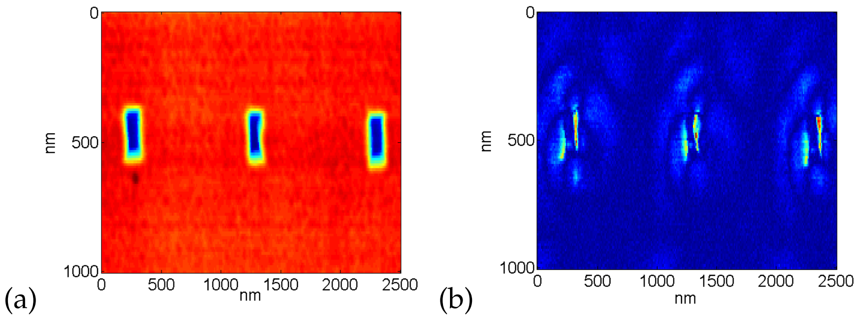

Figure 3.4: (a) AFM image of the nanoslit, fabricated with Focused Ion Beam (FIB) on 40nm of gold. (b) Optical signal due to excitation with 633nm wavelength, polarized horizontally.

3.4.2 *nano-FTIR Measurements*

In order to extract the full spectrum of optical metamaterials we used the nano-FTIR module combined with an ultra-broadband 6 fs laser pulse.

Figure 3.5 shows a typical measuremeant in the nano-FTIR. After normalizing the signal according to equation 2.2, we can see a clear distinction between the nearfield measurement in different point in space. Enhanced optical signal can be seen at the edge of the nano-bar, indicating high spectral response around the wavelength of 960nm.

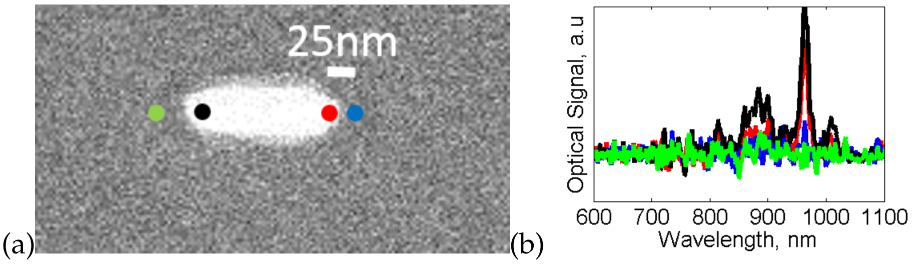

Figure 3.5: (a) A SEM image of a 180nm gold nanobar. (b) Optical Signal as a function of wavelength measured with the nano-FTIR taken at different points. The spectrum at the red and black points show strong optical response around 962nm, while the spectrum taken only 25nm away from the bar (blue and green points) show no observable spectral response.

In order to show consistency in the nano-FTIR measurements, an array of bars with a gradient of lengths was fabricated (Figure 3.6) and a 1-dimensional nano-FTIR measurement was done across the bars' gradient (Figure 3.6, a). The optical signal of different wavelengths in space clearly shows how bars with different aspect-ratio exhibit different optical response, with sub-wavelength resolution. In sub-figures 3.6 (d)-(e) we can clearly see the redshift in the spectrum of nanobars as their aspect ratio grows, just as observed in the far-field in figure 3.2.

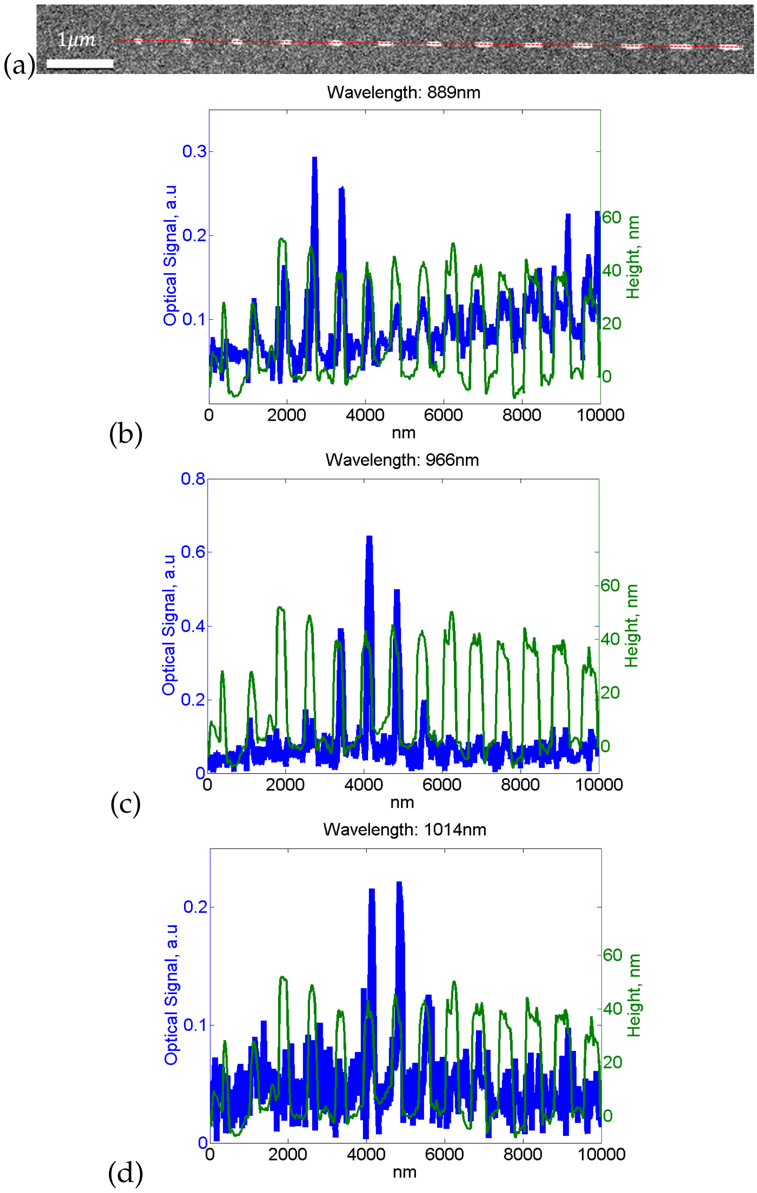

Figure 3.6: (a) SEM image of the nanobars' gradient. A one-dimensional nano-FTIR scan was conducted along the dotted red line. The scan was done across $10\mu m$, with $25nm$-steps. (b)-(d) AFM (Right y-axis, in green) and Optical Signal (Left y-axis, in blue) as a function of *space* for selected wavelengths - 889nm, 966nm and 1014nm. A clear correlation between the nanobars' location in the AFM and their optical signal can be seen. The Strongest optical signal in (b) corresponds to the 140nm nanobar, in (c) to the 180nm long nanobar and in (d) to the 200nm long bar.

Moreover, we have been able to retrieve the second mode of a long bar which resonates around ~1500nm, can be observed at 855nm (Figure 3.7, f). This is unique, as this mode is not observed in the far field, most probably due to it's symmetry, which leads us to the conclusion that it is probably excited by the near-field of an SPP launched in the s-SNOM tip.

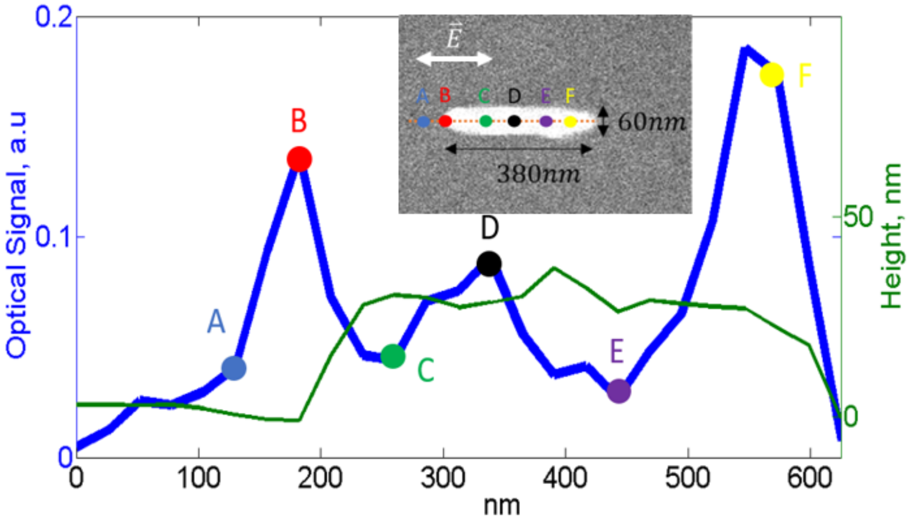

Figure 3.7: The 2^{nd} mode of a gold nanobar. AFM (Right y-axis, in green) and Optical Signal (Left y-axis, in blue) in the wavelength of $855nm$, for a 1-dimensional n-FTIR scan, containing 25 points of measurement with a spacing of $25nm$ (see dotted line in the SEM image). Small image contains a SEM image of a similar bar.

Obtaining these results confirms a unique capability, enabling us to measure a hyper-spectral response with a resolution of 25nm, using a femtosecond laser and an s-SNOM.

4

ULTRAFAST MEASUREMENT FASTER THAN THE SINGLE-CYCLE - THEORY

So far we have explained how information about temporal dynamics can be extracted in a pump-probe experiment. Yet, using an electromagnetic pulse as a temporal shutter can only be used to investigate procceses which are slower than the main frequency of the pulse. In order to investigate processes which are much faster than the single cycle a probe pulse of higher frequency can be employed, complicating the experimental apparatus. Furthermore, if the processes take place in time scales of attoseconds, the probe pulse must compose UV spectral components, which interact strongly with matter due to electronic resonances, damaging it and altering it's optical response. Events which occur on time intervals shorter than a single cycle, such as the oscillations of electron in metals as a result from an incoming electromagnetic pulse, semi-metallization of dielectrics [21], second harmonic generation in nanostructures [22] and Kerr effect [23] are difficult to measure, and understanding their dynamics is motivated both by fundamental science and possible future applications [24][25].

Different methods for investigating the time-dependent polarization of metals with faster than the single cycle resolutions were proposed. These methods incorporate the use of ultrafast pulses of electrons and Transmission Electron Microscope (TEM). Deflection of electrons as a result from the excited nearfield of the metal is recorded as a function of the time delay between the exciting electromagnetic pulse and the electrons' pulse, giving a complete space-time informatiom about the local polarization of the metal. For various reason, the spatio-temporal resolution of these experiments didn't yet exceed the $\sim 1\mu m$-$80fs$ spatio-temporal time scales [26]. Furthermore, probing metal structures with a TEM has two main disadvantages: electron induced damage to the sample due to the energetic electrons and the ability to probe only free-standing structure.

In the next section we propose an experimental apparatus and analysis from which the spatio-temporal near-field polarization can be extracted with a resolution of 25nm and less than a femtosecond, using an s-SNOM and a well characterized ultrafast electromagnetic pulse. Moreover, we present preliminary results, in the near-field and far-field, confirming energy transfer between coupled LSPRs. Future measurements and analysis are dicussed.

4.1 TIME DYNAMICS INFORMATION IN THE INTERFEROGRAM

As we've seen in chapter 2 (*Theoretical Background*), a measurement of an interferogram results in the following quantity:

$$< I(d) >_t = \sum_k |S_k R_k| e^{-i\phi_{s,k}} e^{ikd} \tag{4.1}$$

Let us denote the spatial resolution of the interferogram, containing a discrete number of points, as $\triangle x$. This resolution depends solely on the piezo-electric crystal which translates the reference arm's mirror. A good piezo electric crystal can move the mirror in steps as small as a few nanometers, and even less. To extract information from an interferogram, a Fourier Transform is employed:

$$I_k = |R_k S_k| e^{-i\phi_{s,k}}$$

The resolution, in k-space, will be $\triangle k = \frac{1}{N\triangle x}$, where N is the number of measurement points in the interferogram.

Usually, at this point the analysis of the interferogram comes to a halt. The amplitude and the phase of each Fourier component can be normalized and information regarding the spectral behaviour is presented and analyzed.

We will take it a step further: Let us remember that if we knew all the information about S_k, it's amplitude and phase, we could completely reconstruct the signal in space. That is, completely reconstruct $S(x)$. If we had the spectral phase of the exciting pulse, $\phi_{p,k}$ (see equation 2.5 for details), which cannot be retrieved using an FTIR, we could completely reconstruct $S(x)$ in the following way:

$$S(x) = \sum_k |S_k| e^{i(\phi_{s,k}+\phi_{p,k})} e^{ikx} = \sum_k \frac{I_k^*}{|R_k|} e^{i\phi_{p,k}} e^{ikx}$$

$\phi_{p,k}$ can be retrieved using a FROG and $|R_k|$ can be directly measured by conducting a nano-FTIR measurement on a completely reflecting substrate, such as a gold layer.

The resolution of the signal in space will now be $\triangle x' = \frac{1}{\frac{N}{N\triangle x}} = \triangle x$, which can be as small as a few nanometers. Let us now recall that the signal we are refering to is actually the nearfield of the substrate, which we transformed to a traveling wave. If we wish to gain information on the temporal dynamics of the point in space for which the interferogram was taken, all we need is to transform into the time domain:

$$S(t) = S(-\frac{x}{c}) = \sum_k \frac{I_k^*}{|R_k|} e^{i\phi_{p,k}} e^{-ickt} \tag{4.2}$$

The temporal resolution of the signal is now $\triangle t = \frac{\triangle x}{c}$. For $\triangle x = 100nm$, we will get $\triangle t \approx 330 \times 10^{-18} second \approx 0.3fs$. That is, with only a modest resolution of the displacement of the reference mirror, our temporal resolution can exceed the single cycle of NIR light by one order of magnitude.

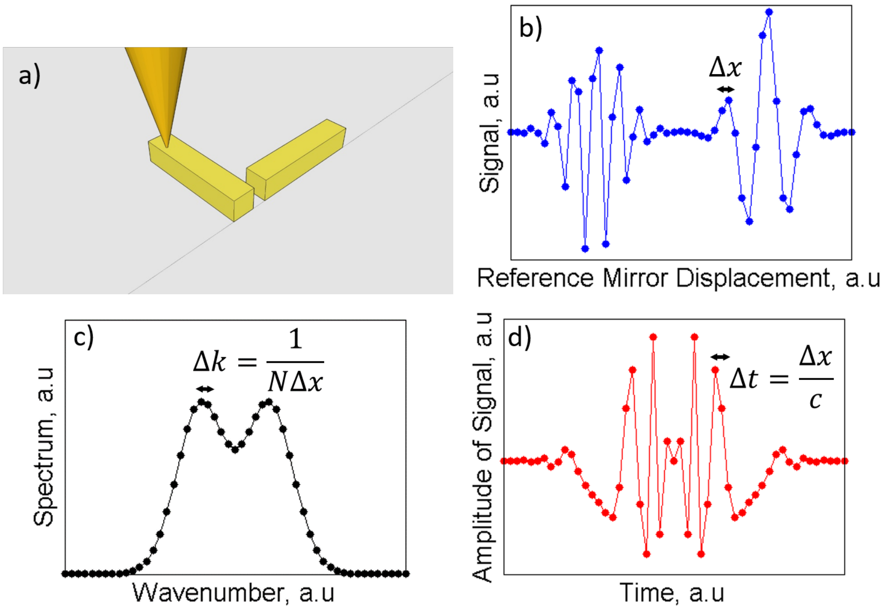

Figure 4.1: Schematics of our proposed method, by order. (a) The tip is placed over a point in the sample. (b) Sweeping the reference mirror with a resolution of $\triangle x$, for N points in space, yields an interferogram. (c) The interferogram is decomposed to it's Fourier components (see equation 4.1), yielding a spectrum with a resolution of $\triangle k = \frac{1}{N\triangle x}$. (d) The spectrum, along with FROG measurements, allows us to reconstruct the signal in time (see equation 4.2). The resolution in the time domain will then give $\triangle t = \frac{\triangle x}{c}$. Additional points in the samples can be measured, giving complete spatio-temporal information on the sample's physics.

4.2 POSSIBLE APPLICATIONS

In the last section, we have shown how an s-SNOM, an ultrafast well-characterized laser pulse and a nano-FTIR can be incorporated. In this section, we will discuss the different configurations in which this system may be used and possible difficulties.

Temporal Dynamics in Coupled LSPRs

A possible configuration of coupled orthogonal gold nano-bars (see figure 4.2). An incident electromagnetic pulse polarized along the x-axis excites the horizontal bar, unaffecting the vertical bar's polarization. The nearfield of the horizontal bar then interacts with the vertical bar, causing to it's polarization and a flow of energy from one bar to the other. Using our method for sub-cycle polarization imaging, we postulate we will be able to extract these dynamics of coupled LSPRs.

Propagation of Surface Plasmons along Nanowires

Further configuration that can be explored: SPP propagation along nanowires due to femtosecond pulse. Different physical parameters, such as dispersion relation, group velocity and average collision time can be extracted. We speculate that this method could be further generalized and used to investigate the femtosecond response of many other 2D materials, which gained significant attention in the last two decades due to their interesting electronic properties.

4.3 MISSING INFORMATION AND ERRORS

Extracting the temporal information in the nearfield, as we explained in this chapter, requires the incorporation of different measurements apparatuses - the s-SNOM, the femtosecond laser and the FROG. These different devices contribute, each, to errors in our final integrated data. The next section discusses the errors and possible artifacts of this method.

4.3.1 *Missing Information due to Non-linear Processes*

As we see in equation 4.2, Fourier components that do not exist in our reference beam will not be observed in the interferogram, even if they exist in the signal beam. These sorts of components may come about as a result of non-linear proccesses.

While proccesses such as Four Wave Mixing (FWM) which may result in an already existing frequency can be accounted for in our methods, other proccesses such as Second Harmonic Generation (SHG) and Third Harmonic Generation (THG) cannot be accounted for. Since these procceses are extremely unefficient, with a second order non-linear susceptibility on the order of magnitude of $\sim 10^{-10}\frac{m}{Volt}$, we suggest that our method will still yield good approximation for the time dynamics of our nanostructures.

4.3.2 *FROG Spectral Phase Retrieval*

Conducting FROG measurements with a well-aligned setup, with no systematic errors, can yield results with errors on the order of magnitude of 10^{-4} [20] for pulses over 10 fs. Below the 10 fs, dispersion that arises due to propagation in the non-linear crystal may result in significant artifacts. If these artifacts cannot be modelled accurately, then using the phase retrieved from the FROG will result in inaccurate measurements. If no systematic artifacts occur, the FROG can yield results with "essentially infinite temporal resolution" [18, 20, 27].

4.3.3 *Errors Originating in the Experimental Apparatus*

Two more factors which can contribute to errors are the displacement of reference mirror and the measurement of intensity in the photodiode. Taking these errors in account can be done by evaluating the errors of a Fourier Transform of an experimental measurement. Further calculations are needed in order to asses the impact of these errors on the final results.

A preliminary calculation which tries to asses these errors can be found in the appendix.

4.4 PRELIMINARY RESULTS - ULTRAFAST DYNAMICS IN LSPRS

This section shows experimental results verifying the method presented at Chapter 3. Our goal was to demonstrate how ultrafast dynamics, with a resolution greater than the single-cycle, can be measured using single well-characterized broadband electromagnetic.

4.4.1 *Time Domain Simulations of Coupled LSPRs Dynamics*

In order to simulate the effects of nanostructures in the time domain an FDTD (*Lumerical*) software was employed. A configuration of orthogonal bars was simulated and the electric field at different point in space was extracted as a function of time. The simulations clearly show a delay of ~5 femtosecond between the maximum excitation of each neighbouring bar. Furthermore, "returning" oscillations can be seen in the first bar after ~10 femtosecond (data not shown), corresponding to an analogue of two conjugated harmonic oscillators, where only one oscillator is excited.

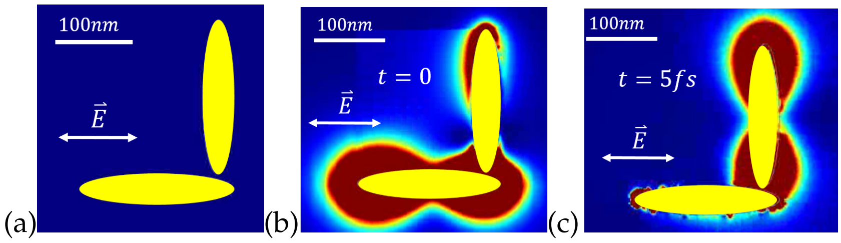

Figure 4.2: (a) The suggested configuration for 2 orthogonal gold nanobars. (b)-(c) Lumerical (FDTD) time domain simulation of the electric near field enhancement in the suggested configuration, as a result of excitation of a 6 fs pulse polarized in the x-axis. At the beginning the pulse excites only the horizontal bar, since it's LSPR can only be excited by x-axis polarized light. After ~5 fs, energy is transferred from the horizontal bar to the vertical bar due to nearfield interaction.

4.4.2 *Experimental Measurements of Coupled Orthogonal Bars*

Arrays of orthogonal bars, with different spacings were fabricated using Electron Beam Lithography. An example of a fabricated nanostructure can be seen in figure 4.3.

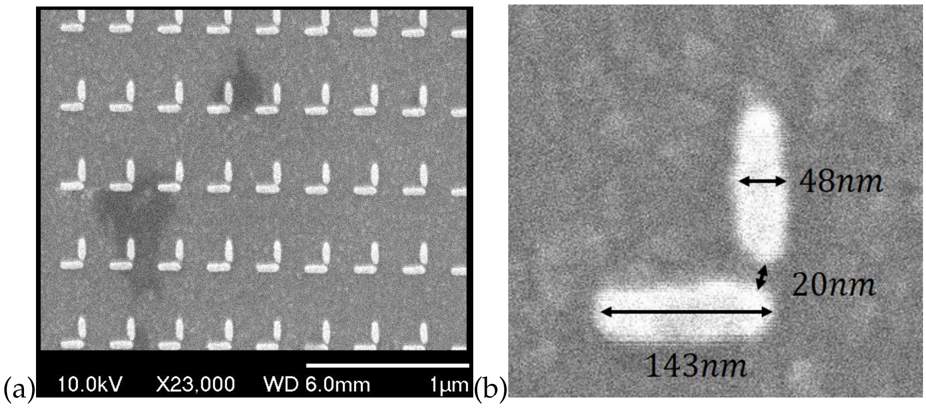

Figure 4.3: (a) SEM image of an array of coupled orthogonal bars. (b) Close up on a single nanostructure.

4.4.2.1 *Far field Characterization*

Arrays were characterized in the far-field using a Transmission/Reflection setup.

In order to qualitatively assess the strength of the coupling we conducted the characterization as follows: x-axis polarized light was shined on the sample, thus exciting the horizontal the horizontal nanobar. After light collection a y-polarizer was set before the spectrometer, thus only light which originated from the scattering of the vertical bar is measured. Figure 4.4 shows the y-polarized light of a few selected arrays, indicating a clear energy transfer between the horizontal and vertical nanobars.

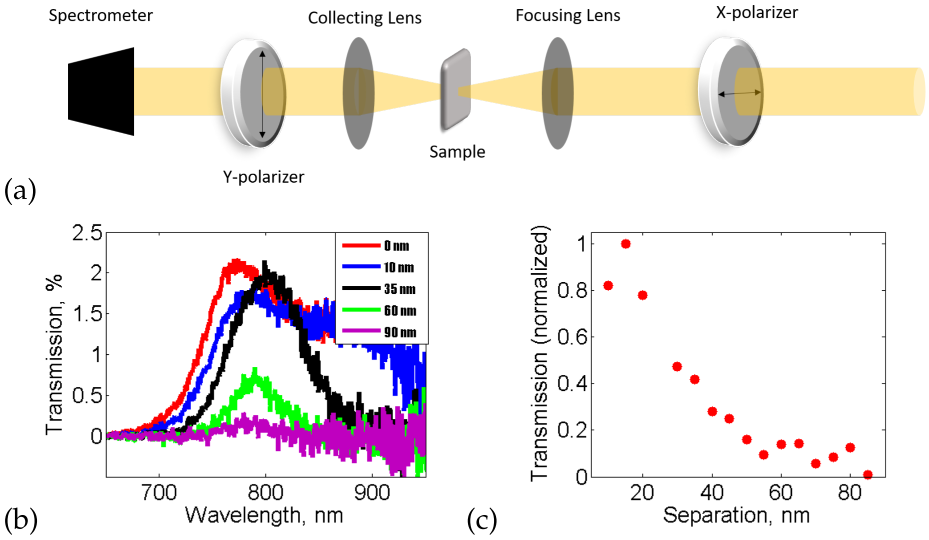

Figure 4.4: (a) Schematics of the characterization setup employed in order to measure the transfer of energy between the nanostructures. (b) The y-polarized scattering of selected arrays of orthogonal bars with different spacings. (c) Y-polarized scattering vs. the separation between the nanobars. The data clearly shows of separation-dependent coupling in the adjacent nanobars.

Nearfield Measurements

Sample was characterized with a broadband Ti:sap fs laser, 650-1100nm. Figure 4.5 shows the optical signal as a function of space for coupled and uncoupled orthogonal bars, for incident light polarized in the x-axis. As can see in the case of uncoupled bars (Sub-figures (a) and (d)), the nearfield optical signal is concentrated on the horizontal bar alone (point A). When the bars are coupled (Figure 4.5, sub-figures (b) and (d)), excitation of the horizontal bar (point A) and vertical bar (points B and C) can be seen, confirming that an energy transfer from the horizontal bar to the vertical bar does exist, as the far-field measurements have shown.

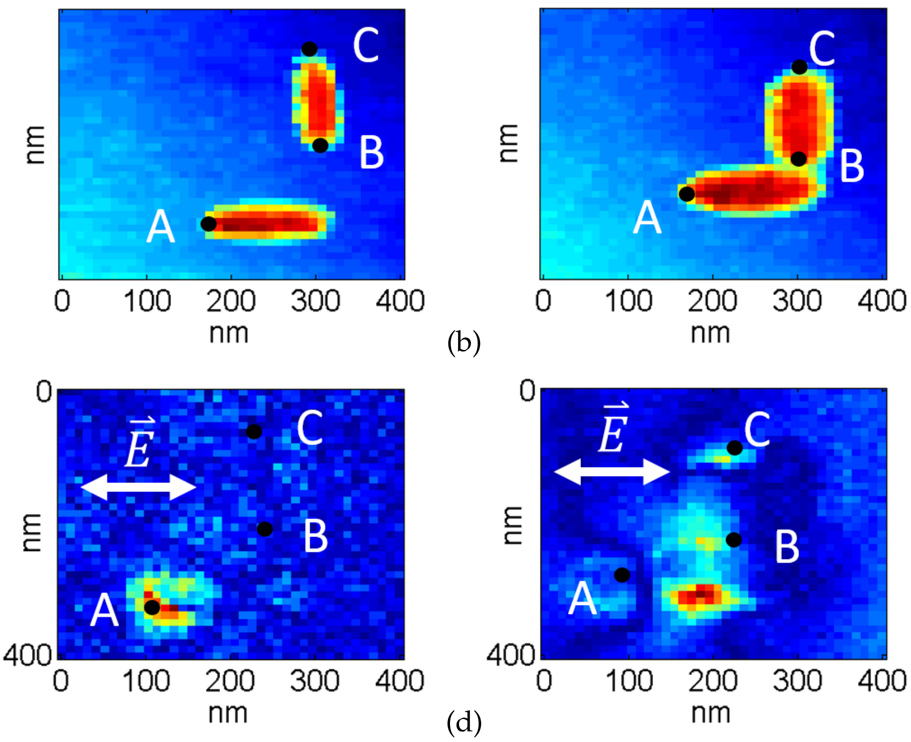

(a) (b) (c) (d)

Figure 4.5: (a) AFM image of uncoupled bars. (b) AFM image of coupled bars. (c) Nearfield Optical signal of the uncoupled orthogonal bars. (d) Nearfield Optical signal of the coupled orthogonal bars.

The next step will be taking an interferogram from each point in space. By adding the spectral phase measured in the FROG to the data we will acquire in the nano-FTIR, and following the mathematical analysis detailed in equation 4.2, we will be able to completely reconstruct the signal in space and time with deep sub-wavelength sub-single cycle resolution. We predict that this analysis will yield similar results to those obtained in numerical simulations such as in figure 4.2, in which energy transfer of a few femtoseconds can be observed.

SUMMARY

In the last chapter we introduced a method we predict will enable spatio-tempral measurement of nanoparticles' polarization with deep subwavelength spatial resolution and sub-cycle temporal resolution. We introduced an example of nanobars configurations with a clear expected temporal dynamics, and have proven that this coupling indeed exists in the far-field and in the near-field. Future near-field measurements, which will include phase and spectrum of each point in space will allow us to fully reconstruct these dynamics in the nearfield domain. Furthermore, a better understanding the uncertainties of this method needs to be achieve by direct calculation of the expected errors.

While the linear response of gold is quite well-understood, the optical properties of many 2D materials frequenctly unknown. By confirming an ability to probe the dynamics of polarization in the nearfield with sub-cycle resolution, we hope to apply this method in the future to study other exotic 2D materials.

5

SUMMARY AND OUTLOOK

The Nano-Femto world spans many of nature's fundamentals processes - from the vibration of molecules to the oscillations of electrons in metals. Since it's processes take place below the diffraction limit and faster than the typical electronic resolution, it's investigation requires the employment of novel methods.

In my M.Sc thesis I have shown how the oscillations of electrons in nanoparticles, LSPRs, can be studied by employing an s-SNOM and an ultrafast femtosecond laser. I extract the spectral response of gold nanostructures with a resolution of 25nm, as well as spatially characterize different modes of the LSPRs. Furthermore, I've measured energy transfer between nanostructures on the nanoscale.

In order to investigate these processes in the time domain, we have introduced a theoretical method which can reconstruct the signal in space and time with a temporal resolution higher than the single cycle, by incorporating the nano-FTIR and FROG. We propose that this method can be used also for the investigation of SPPs in metals and other polariton dynamics in 2D materials. An ongoing work tries to verify this method.

Future experiments are planned in order to verify this method experimentally on coupled configurations of LSPRs. After verification we plan to demonstrate that this method can be used on other materials.

Further experiments will also include Surface Enhanced Raman Scattering (SERS), Tip Enhanced Raman Scattering (TERS) in the s-SNOM, coherent control in the s-SNOM using Spatial Light Modulator (SLM) and coupling of different molecules to metallic nanoparticles.

APPENDIX

FABRICATION

Design of nanostructures was done with Raith150 *software* and *Raith GDSII* Toolbox. In order to fabricate nanostructure with nanometric resolution two main methods were applied: Electron Beam Lithography and Focused Ion Beam. The followings are the details of the procedures.

Electron Beam Lithography

ITO coovered glass (*Sigma-Aldrich,* $70-100\frac{\Omega}{sq}$) were spin-coated in 6500 RPM with *PMMA-A4* polymer for 1 minute, following with a one minute heating in $180\mathring{C}$. Writing was conducted using a 20kV, $20\mu m$ aperture, 6mm WD beam, and a dose of $\sim 500\frac{pC}{cm}$ was deposited in single-line pixels, in steps of 4 nm. Sample was then developed for 1 minute in MIBP/IPA 1:3, and rinsed in Isopropanol for 20 seconds. Samples were then cleaned in Oxygen plasma, $\sim 50kW$, for 12 seconds.

Gold was evaporated in a rate of $0.5\frac{\AA}{sec}$in a thermal evaporator, following lift-off in Acetone and a final rinse in Isopropanol. Samples were then inspected in a SEM for final results.

An example of the final product can be seen in figure 5.1.

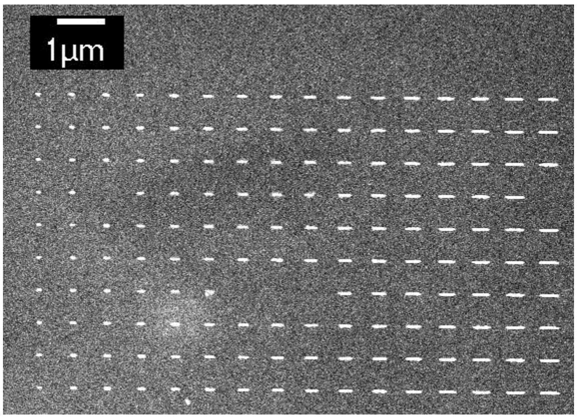

Figure 5.1: SEM image of gold nanobars, fabricated with E-Beam lithography.

Focused Ion Beam (FIB)

Gold was evaporated in a rate of $0.5\frac{Å}{sec}$ in a thermal evaporator on bare glass. Writing was done with a 35kV, $30\mu m$, 7 pA beam. Samples' inspection was then conducted in a SEM.

ERRORS IN THE EXPERIMENTAL APPARATUS

This section wishes to give asses the errors in the Fourier Transform of an interferogram.

Estimation of Errors of a Fourier Transform

Let I_d be the interferogram of a signal f. Assuming the interferogram is discrete with N points, it can be shown the the amplitude at the i_{th} point of measurement is:

$$I_{x_i} = \frac{1}{\sqrt{N}} \sum_k f_k e^{ikx_i}$$

The frequency components in f can be calculated by implementing a Fourier Transform:

$$f_k = \frac{1}{\sqrt{N}} \sum_{i=1}^{N} I_{x_i} e^{-ikx_i}$$

We can see that there might be two different contributions to the errors of the Fourier Transform - the error in I_{x_i}, which we will denoted as $\triangle I$, and the error in the displacement of the reference mirror, x_i, which we will denote as $\triangle x$ (in our system. Approximating these errors can be done using the partial-derivatives method.

Assuming the error in the intensity is the same for all measurement points in the interferogram we can approximate the error in f_{k_j} by the partial-derivatives method in the following way:

$$\triangle f_{k_j} = \frac{\triangle I_x}{\sqrt{N}} \sum_{i=1}^{N} e^{-ik_j x_i}$$

Repeating this procedure for the displacement errors, $\triangle x_j$, yield:

$$\triangle f_{k_j} = \frac{(-ik_j \triangle x)}{\sqrt{N}} \sum_{i=1}^{N} f_{k_j} e^{-ik_j x_i}$$

We can now give an upper bound to these erros in the amplitude and phase:

$$\triangle|f_{k_j}| = |\frac{\triangle I_x}{\sqrt{N}}\sum_{i=1}^{N} e^{-ik_j x_i}| + |f_{k_j} k_j \triangle x| \leq |\sqrt{N}\triangle I_x| + |f_{k_j} k_j \triangle x|$$

Calculating the upper boundary for the phase of f_{k_j}, $\phi_{k_j} = -i \times ln(f_{k_j})$, will yield:

$$|\triangle\phi_{k_j}| = |\frac{\triangle I_x}{\sqrt{N}} \frac{\sum_{i=1}^{N} e^{-ik_j x_i}}{f_{k_j}}| + |k_j \triangle x| \leq |\frac{\sqrt{N}\triangle I_x}{f_{k_j}}| + |k_j \triangle x| \quad (5.1)$$

Estimating the Errors in Time

As we have seen in *Chapter 4*, the phase ϕ_{k_j} allows us to extract the time dynamics in our sample. Thus, understanding the different contributions to it's errors is of great importance.

As we've seen in equation 5.1, there are two contribution to phase errors. The first time, arrising from the uncertainty in the intensity. Assuming a 1,000-points interferogram with an SNR of 0.01, the error in the phase will be $\triangle\phi_{k_j} \sim 0.3$ radians. The second one, arrising from the uncertainty in the movement of the reference mirror is $k_j \triangle x$, where k_j is the wave-vector and $\triangle x$ is the uncertainty in the reference mirror's displacement. For a wavelength of $850nm$ and $\triangle x = 6nm$ we will get an error in the phase of ~ 0.04 radians. Assuming a reasonable SNR, our error in the phase will be $\triangle\phi_{k_j}$ will be ≤ 0.3 radians.

Transforming to the time domain, a delay in the signal between two points can be approximated by the slope of the phase. Let two points have a linear measured phase a_1 and a_2, respectively. In that case, the delay in time will be:

$$t_2 - t_1 = \frac{a_2 - a_1}{c} \pm \frac{\triangle a_1 + \triangle a_2}{c}$$

Thus, by understanding the uncertainty in the slopes of the phase we can give an assesment to the errors in the time domain.

Further experimental measurements are needed in order to precisely asses these uncertainties.

BIBLIOGRAPHY

[1] Mie Gustav. “Contributions to the optics of turbid media, particularly of colloidal metal solutions.” In: *Annalen der Physik* (1908) (cit. on p. 1).

[2] Jwa-Min Nam, C. Shad Thaxton, and Chad A. Mirkin. “Nanoparticle-Based Bio-Bar Codes for the Ultrasensitive Detection of Proteins.” In: *Science* 8.2 (2003), pp. 18–24 (cit. on pp. 1, 6).

[3] Marc Vendrell, Kaustabh Kumar Maiti, Kevin Dhaliwal, and Young-Tae Chang. “Surface-enhanced Raman scattering in cancer detection and imaging.” In: *Trends in Biotechnology* 17.12 (2013), pp. 667–673 (cit. on pp. 1, 6).

[4] Jennifer P. Leung, Keng C. Chou Sherry Wu, and Ruth Signorell. “Investigation of Sub-100 nm Gold Nanoparticles for Laser-Induced Thermotherapy of Cancer.” In: *Nanomaterials* 17.12 (2013), pp. 667–673 (cit. on p. 1).

[5] Amit Agrawal, Rajesh Deo, Geoffrey D. Wang, May D. Wang, and Shuming Nie. “Nanometer-scale mapping and single-molecule detection with color-coded nanoparticle probes.” In: *PNAS* 17.12 (2007), pp. 667–673 (cit. on pp. 1, 6).

[6] Sergey Makarov, Sergey Kudryashov, Ivan Mukhin, Alexey Mozharov, Valentin Milichko, Alexander Krasnok, and Pavel Belov. “Tuning of Magnetic Optical Response in a Dielectric Nanoparticle by Ultrafast Photoexcitation of Dense Electron Hole Plasma.” In: *Nano Letters* 17.12 (2015), pp. 667–673 (cit. on pp. 1, 6).

[7] Martti Kauranen and Anatoly Zayats. “Nonlinear Plasomnics.” In: *Nature Photonics* 17.12 (2012), pp. 667–673 (cit. on p. 1).

[8] Brian R. Saunders and Michael L. Turner. “Nanoparticle-polymer photovoltaic cells.” In: *Advances in Colloid and Interface Science* 17.12 (2008), pp. 667–673 (cit. on p. 1).

[9] Yongmin Liu and Xiang Zhang. “Metamaterials: a new frontier of science and technology.” In: *Chem. Soc. Rev.* 17.12 (2011), pp. 667–673 (cit. on p. 1).

[10] Augustine M Urbas, Zubin Jacob, Luca Dal Negro, Nader Engheta, A D Boardman, P Egan, Alexander B Khanikaev, Vinod Menon, Marcello Ferrera, and Nathaniel Kinsey. “Roadmap on optical metamaterials.” In: *Journal of Optics* 17.12 (2016), pp. 667–673 (cit. on p. 1).

[11] HC van de Hulst. *Scattering by Small Particles*. Dover publications. 1981 (cit. on p. 5).

[12] E. Prodan and P. Nordlander. “Plasmon hybridization in spherical nanoparticles.” In: *The Journal of Chemical Physics* (2004) (cit. on p. 6).

[13] P. Nordlander, C. Oubre, E. Prodan, K. Li, and M. I. Stockman. “Plasmon Hybridization in Nanoparticle Dimers.” In: *Nano Letters* 17.12 (2004), pp. 667–673 (cit. on p. 7).

[14] Naomi J. Halas, Surbhi Lal, Wei-Shu Chang, Stephan Link, and Peter Nordlander. “Plasmons in Strongly Coupled Metallic Nanostructures.” In: *Chemical Reviews* (2011) (cit. on p. 7).

[15] Florian Huth. *Nano FTIR - Nanoscale Near-Field Infrared Spectroscopy*. PhD Thesis. 2015 (cit. on p. 8).

[16] Nenad Ocelic, Andreas Huber, and Rainer Hillerbrand. “Pseudoheterodyne detection for background-free near-field spectroscopy.” In: *Applied Physics Letters* 17.12 (2006), pp. 667–673 (cit. on pp. 9, 17).

[17] Symner P. Davis, Mark C. Abrams, and James W. Brault. *Fourier Transform Spectrometry*. Academic Press. 2001 (cit. on p. 11).

[18] Kenneth W. DeLong, David N. Fittinghoff, and Rick Trebino. “Practical Issues in Ultrashort Laser-Pulse Measurement Using Frequency-Resolved Optical Gating.” In: *IEEE Journal of Quantum Electronics* 17.12 (1996), pp. 667–673 (cit. on pp. 12, 25).

[19] Andrew M. Weiner. “Ultrafast optical pulse shaping: A tutorial review.” In: *Optics Communication* 17.12 (2011), pp. 667–673 (cit. on p. 12).

[20] Rick Trebin, Kenneth W. DeLong, David N. Fittinghoff, John N. Sweetser, Marco A. Krumbügel, Bruce A. Richman, and Daniel J. Kane. “Measuring ultrashort laser pulses in the time-frequency domain using frequency-resolved optical gating.” In: *Review of Scientific Instruments* 17.12 (1998), pp. 667–673 (cit. on pp. 13, 24, 25).

[21] Ojoon Kwon, Tim Paasch-Colberg, Vadym Apalkov, Bum-Kyu Kim, Ju-Jin Kim, Mark I. Stockman, and D. Kim. “Semimetallization of dielectrics in strong optical fields.” In: *Scientific Reports* (2016) (cit. on p. 21).

[22] Roderick B. Davidson, Anna Yanchenko, Jed I. Ziegler, Sergey M. Avanesyan, Benjamin J. Lawrie, and Richard F. Haglund Jr. “Ultrafast Plasmonic Control of Second Harmonic Generations.” In: *ACS Photonics* (2016) (cit. on p. 21).

[23] A. Sommer et al. “Attosecond nonlinear polarization and light-matter energy transfer in solids.” In: *2016* (2016) (cit. on p. 21).

[24] Michael Kruger and Nirit Dudovich. “Resolving the attosecond beat.” In: *Nature Photonics* (2016) (cit. on p. 21).

[25] Ahmed H. Zewail. “4D Ultrafast Electron Diffraction, Crystallography, and Microscopy.” In: *Ann. Rev. Phys. Chem.* (2006) (cit. on p. 21).

[26] A. Ryabov and P. Baum. “Electron microscopy of electromagnetic waveforms.” In: *Science* 17.12 (2016), pp. 667–673 (cit. on p. 21).

[27] Daniel J. Kane and Rick Trebino. “Single-shot measurement of the intensity and phase of an arbitrary ultrashort pulse by using frequency-resolved optical gating.” In: *Optics Letters* 17.12 (1993), pp. 667–673 (cit. on p. 25).

COLOPHON

This document was typeset using `classicthesis` style developed by André Miede. The style was inspired by Robert Bringhurst's seminal book on typography *"The Elements of Typographic Style"*. It is available for LaTeX and LyX at

https://bitbucket.org/amiede/classicthesis/

Happy users of `classicthesis` usually send the author a real postcard; the collection of postcards received so far is featured at

http://postcards.miede.de/

תקציר

מגוון תהליכים בטבע, כגון אוסילציות של אלקטרונים במתכות, ויברציות של מולקולות ותנודות של גלים א"מ בתחום הנראה והאינפרא-אדום מתרחשים בסדרי גודל של ננומטרים (10^{-9} מטר) ופמטו-שניות (10^{-15} שנייה). חקירת תהליכים אלו מהווה אתגר מדעי הדורש יישום של כלים מדעיים המאפשרים רזולוציות זמן-מרחב מעבר לזמן התגובה של אלקטרוניקה רגילה וגבול הדיפרקציה המרחבי של גלים אלקטרומגנטיים.

בעבודה זו אנחנו מדגימים כיצד שילוב בין לייזר פמטו-שנייה רחב סרט (fs laser) ומיקרוסקופ שדה קרוב (s-SNOM) מאפשר מדידת ספקטרום של ננו-חלקיקים עם רזולוציה מרחבית של 25 ננומטר. בנוסף, אנחנו מציגים תיאוריה המאפשרת מעבר מהמדידות הספקטראליות לדינמיקה זמנית, עם רזולוציה הגבוהה מהמחזור הבודד.

הפרק הראשון (Introduction) מציג מבוא לננו חלקיקים פעילים אופטית, וכן לתופעות טבע מהירות במיוחד (Ultrafast phenomena). הפרק השני (Theoretical Background) מציג סקירה תיאורטית ומתמטית בתחומי האינטראקציה בין אור לחומר, עם דגש על פלזמוניקה (Plasmonics), וכן הסבר על מיקרוסקופיית השדה הקרוב (Near-field Microscopy) ופולסים א"מ רחבי סרט. בפרק השלישי (Experimental apparatus) מובאות תוצאות נומריות וניסיוניות של אינטראקציה של ננו-חלקיקים עם אור. בתחילת פרק זה נציג תוצאות מדידות בשדה הרחוק, ובהמשכו נציג תמונות שדה קרוב שנמדדו באמצעות מיקרוסקופ שדה קרוב ואור קוהרנטי מונוכרומאטי. כמו כן, נציג מדידות שנעשו בעזרת לייזר טיטניום-ספיר רחב סרט (650-1100 ננומטר) ומיקרוסקופ השדה הקרוב, בהן ניתן לצפות בספקטרום המלא של ננו-חלקיקים עם רזולוציה מרחבית של 25 ננומטר. לבסוף, פרק 4 (Ultrafast Measurements Faster than the Single Cycle – Theory and Preliminary Results) מציג תיאוריה המאפשרת להתמיר את המדידות הספקטראליות לדינמיקה זמנית עם רזולוציה גבוהה מהמחזור הבודד. בפרק זה נציג תוצאות ראשוניות, ונדון במדידות נוספות (שטרם בוצעו) הנדרשות להוכחת התיאוריה באופן ניסויי. כמו כן, נדון בשימושים אפשריים נוספים לשיטה זו בחקר חומרים דו-מימדיים.

TEL AVIV UNIVERSITY
אוניברסיטת תל אביב

הפקולטה למדעים מדויקים ע"ש ריימונד ובברלי סאקלר

בית הספר לפיסיקה ואסטרונומיה

המחלקה לחומר מעובה

תגובה אופטית רחבת-סרט של ננו-מבנים פלזמונים עם רזולוציה מרחבית מעבר לגבול הדיפרקציה

חיבור זה מוגש כחלק מהדרישות לקבלת תואר 'מוסמך למדעים' באוניברסיטת תל אביב

על ידי

אורי אריאלי

עבודה זו הוכנה בהנחיתו של

ד"ר חיים סוכובסקי

מרץ 2017